Acta Cryst. (1984). B40, 115–125

New Series of Superstructures Based on a Clinopyroxene. I. The Structure of the 'Enstatite-IV' Series, $[Mg_{(x-12)/3}Sc_4][Li_{4/3}Si_{(x-4)/3}]O_x$, with $x = 100$, 112 or 124

BY YOSHIO TAKÉUCHI AND YASUHIRO KUDOH

Mineralogical Institute, Faculty of Science, University of Tokyo, Hongo, Tokyo 113, *Japan*

AND JUN ITO*

James Franck Institute, University of Chicago, Chicago, IL 60637, *USA*

(*Received* 14 *October* 1983; *accepted* 15 *November* 1983)

Abstract

The chemical series called 'enstatite-IV' (En-IV), $[Mg_{(x-12)/3}Sc_4][Li_{4/3}Si_{(x-4)/3}]O_x$, comprises three subphases: En-IV-10, En-IV-9, and En-IV-8. Crystal data: En-IV-10: $a = 9{\cdot}429(2)$, $b = 8{\cdot}748(2)$, $c = 27{\cdot}038\ (8)$ Å, $\beta = 93{\cdot}25\ (2)°$, $P2/a$, $Z = 1$, $x = 124$; En-IV-9: $a = 9{\cdot}432\ (2)$, $b = 8{\cdot}756\ (1)$, $c = 48{\cdot}792\ (14)$ Å, $\beta = 92{\cdot}25\ (2)°$, $I2/a$, $Z = 2$, $x = 112$; En-IV-8: $a = 9{\cdot}429\ (2)$, $b = 8{\cdot}741\ (1)$, $c = 21{\cdot}808\ (6)$ Å, $\beta = 91{\cdot}20\ (2)°$, $P2/a$, $Z = 1$, $x = 100$. Their structures bear superstructure relations to a *C*-centred clinopyroxene (CPX) and consist of cuts (or slabs), parallel to $(10\bar{1})$, of the CPX structure, the cuts being 10-tetrahedra wide for En-IV-10, and 9- and 8-tetrahedra wide for En-IV-9 and En-IV-8, respectively. Each cut in the structures of En-IV-10 and En-IV-8 is related to its adjoining cuts by an **a**/2 glide, while that in En-IV-9 is by a **b**/2 glide. The silicate chains in the cut retain their continuity through tetrahedra, denoted *T*, which occur at the boundaries; *T* play a role which is similar to that of the offset tetrahedra in pyroxenoids. The contents of Sc at the cation positions of the slab show the general trend that they increase as the positions approach to the slab boundaries. As the difference in structure type is related to the Sc/(Mg + Sc) ratio, the structure series provides an example of tropochemical cell-twinning of the CPX structure; with $(10\bar{1})$ as the twin plane and glides of either **a**/2 or **b**/2 as the twin operation. The lower the Sc/(Mg + Sc) ratio, the less frequent the cell-twinning.

Introduction

Among three pyroxenes that exist at 1523 K in the system $MgSiO_3$–$LiScSi_2O_6$ (Ito & Steele, 1976), the protoenstatite solid solution occurs in the range of the $MgSiO_3$ (enstatite) component from about 60 up to 95 mol%. It is unquenchable if that component exceeds 95 mol%. At temperatures above those of the protoenstatite field, the existence of a new phase was discovered by one of the authors (the late Jun Ito), the liquids of the phase existing between 1823 ~ 1658 K (Ito & Steele, 1976). Below about 1673 K, this phase is decomposed into the protoenstatite type (Fig. 1). Noting that three well characterized structure types are known for enstatite, we called the new phase 'enstatite-IV' and denoted it En-IV (Takéuchi, Kudoh & Ito, 1977). This, however, does not necessarily imply that the compositional range of En-IV extends up to the very pure composition of $MgSiO_3$. The crystal structure of $MgSiO_3$ at around 1673 K has been studied by Murakami, Takéuchi & Yamanaka (1984).

The En-IV phase in fact consists of a series of subphases, each bearing a superstructure relation to a clinopyroxene [a diagram showing subphase relations has been proposed by J. Ito and given in Takéuchi (1978)]. Three basic subphases which have been found to date have been denoted En-IV-8, En-IV-9, En-IV-10 in increasing order of the contents of the $MgSiO_3$ component. Note that these symbols are revised versions of En-IV-22, En-IV-20, and En-IV-18, respectively, which we used previously (Takéuchi, 1978). The meaning of the Arabic figures which follow En-IV will be given below. Another superstructure series can be obtained which is similar to En-IV but free from Li. We call it the Sc series of En-IV.

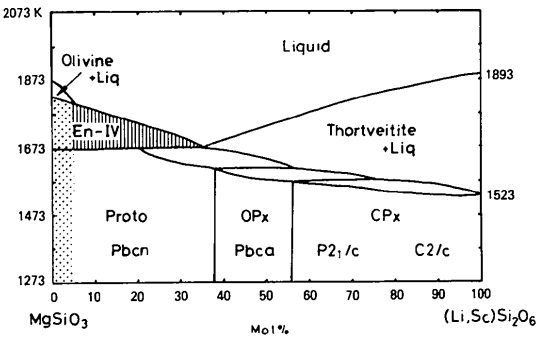

Fig. 1. The phase relation in the $MgSiO_3$–$LiScSi_2O_6$ system above 1273 K, the ruled area showing the En-IV field. The nonquenchable composition region is stippled.

* Deceased 6th June 1978.

0108-7681/84/020115-11$01.50

These series of superstructures are of particular interest for the following two reasons. First, they occur before the breakdown of the protoenstatite structure type into a melt, and, second, they provide a beautiful example in which the variety in cell dimensions of a superstructure series is controlled by a minor change in chemistry. In fact, the mechanism underlying the formation of these structure series may be regarded as an example of tropochemical cell-twinning (Takéuchi, 1978; Takéuchi, Haga, Kato & Miura, 1978; Takéuchi, Ozawa & Takagi, 1979). The purpose of the present paper is to describe the result of our structural study of En-IV. The structures of En-IV (Sc series) will be discussed at a later date. The following symbols are used here: CPX: clinopyroxene; **M1**: a family of the cation sites which correspond to the $M(1)$ site of a C-centred CPX; **M2**: a family of the cation sites which correspond to the $M(2)$ site of a C-centred CPX. In addition, the symbols **O1**, **O2**, and **O3** have been defined similarly. Brief accounts of the structure of the En-IV series have appeared (Takéuchi *et al.*, 1977; Takéuchi, 1978).

Experimental

Preparation of materials

The starting materials used for the syntheses of the En-IV crystals were Li_2CO_3, Sc_2O_3, MgO, and H_2SiO_3. To obtain the crystals of an En-IV phase, a mixture of these materials in the desired ratio was melted at around 1773 K. After cooling to around 1673 K at a rate of 3–4 K h^{-1}, this was quenched in air. The chemical compositions of the three specimens which were thus prepared and used for the present study are given in Table 1, together with their structure types. Divalent atoms such as Co, Mn, or Zn may be doped in the structure; specimen (2) is an example in which Co atoms were doped. These compositions were provided by electron-microprobe analyses carried out by Dr I. Steele, except for the contents of Li_2O which were obtained by the atomic-absorption method. It is notable that from the chemical composition of specimen (1), in particular, we may derive a formula

$$(Mg_{0\cdot932}Sc_{0\cdot074})_{\Sigma=1\cdot006}(Si_{0\cdot969}Li_{0\cdot028}Mg_{0\cdot003})_{\Sigma=1\cdot000}O_3.$$

The chemical formula thus expressed is almost exactly that of a metasilicate type and one can assume that the following new substitution scheme, rather than $Li + Sc \rightleftarrows 2Mg$, has taken place:

$$\begin{cases} 3Mg \rightleftarrows 3Sc \\ Si \rightleftarrows Li. \end{cases}$$

The structural formulae of the three specimens will be given below together with the principles of the chemical composition of the En-IV series.

Table 1. *Chemical compositions of the three specimens used for the present study*

Specimen	(1)	(2)	(3)
Structure type	En-IV-10	En-IV-9	En-IV-8
Density (g cm^{-3})			
exp.	3·15	3·27	—
calc.	3·13	3·25	3·15
Chemical composition (wt.%)			
SiO_2	58·07	55·69	56·22
Sc_2O_3	5·12	6·68	9·48
Li_2O	0·41	0·53	0·59
MgO	37·53	28·92	33·99
CoO	—	8·30	—
Total	101·13	100·12	100·28

Table 2. *Crystal data of the En-IV series*

	En-IV-10	En-IV-9	En-IV-8
Axes set *A*			
a (Å)	9·429 (2)	9·432 (2)	9·429 (2)
b (Å)	8·748 (2)	8·756 (1)	8·741 (1)
c (Å)	55·416 (16)	50·058 (14)	44·816 (12)
β (°)	103·03 (2)	103·10 (2)	103·34 (2)
V (Å^3)	4453·29	4026·53	3594·02
c length per octahedron (Å)	2·771	2·781	2·801
c length per tetrahedron (Å)	2·519	2·503	2·490
Space group	*B2/a*	*A2/a*	*B2/a*
Axes set *B*			
a (Å)	9·429 (2)	9·432 (2)	9·429 (2)
b (Å)	8·748 (2)	8·756 (1)	8·741 (1)
c (Å)	27·038 (8)	48·792 (14)	21·808 (6)
β (°)	93·25 (2)	92·25 (2)	91·20 (2)
Space group	*P2/a*	*I2/a*	*P2/a*
CPX subcell			
a (Å)	9·801	9·804	9·794
b (Å)	8·748	8·756	8·741
c (Å)	5·542	5·562	5·602
β (°)	110·40	110·44	110·48

Unit cell and space group

The crystals of En-IV are transparent and platy parallel to (001). The monoclinic cell dimensions of the three specimens were obtained with a single-crystal Syntex $P2_1$ diffractometer using graphite-monochromated Cu $K\alpha$ radiation ($\lambda = 1{\cdot}54178$ Å) (Table 2). The relationships between the unit cells of these En-IV phases and their CPX subcells are illustrated in Fig. 2. As will be observed in this figure, there are basically two ways, *A* and *B*, to choose the set of axes for the En-IV series of crystals. In the former case (Table 2), in which the *c* axis of En-IV is parallel to *c* of the CPX subcell, the unit cell of En-IV may simply be expressed as a stack, in parallel position, of N CPX cells along their common *c* axes; N being 10, 9, and 8 for the unit cells of En-IV-10, En-IV-9, and En-IV-8, respectively. The Arabic figure, which follows En-IV in the notation of each structure type, thus corresponds to the number of CPX cells that constitute the unit cell of the structure type. However, note that these figures were originally introduced to represent a more important structural feature of the En-IV series which will be given later. In the *A* choice of axes, there is a simple rule between the

space group and N: if N is even the space group is $B2/a$, and if odd $A2/a$.

In the latter choice of axes (Fig. 2), the unit cell become primitive if N is even, while it becomes body-centred if N is odd (Table 2). Choice A is better for discussing the relationship between the superstructure of En-IV and the CPX structure, while B is geometrically simpler than A particularly if N is even; we used B for the structure determination and the description of the atomic parameters.

Intensity-data collection

The ω–2θ scan technique was used to collect, on the above-mentioned single-crystal diffractometer, the graphite-monochromated Cu $K\alpha$ reflection intensities. Details are in Table 3. Intensities were corrected for Lorentz and polarization factors as well as absorption, the latter being carried out with the computer program *ACACA*, based on the procedure provided by Wuensch & Prewitt (1965).

Structure determination and refinement

The structure analysis was initiated with specimen (1) having a c periodicity of 27·038 Å. For structure determination, those reflections were used whose intensities were greater than $2\sigma(I)$. The three-dimensional Patterson function revealed the notable feature that the CPX substructure had a strong C-centred nature. Consequently, the CPX structure on which the superstructure is based may well be regarded as a C-centred CPX, having space group $C2/c$, such as high clinohypersthene (Smyth & Burnham, 1972). The E maps were then prepared: one was based on 18 reflections whose $|E|$ values were greater than 5·166 and yielded signs of E with probability of 1·000; the other was based on 268 reflections with $|E|>5{\cdot}166$, and signs which had probability higher than 90% (95% on average). These E maps revealed, without ambiguity, arrays of cation positions along lines parallel to [102] and passing through the twofold axes either at $\frac{1}{4}$, y, 0 or at $\frac{3}{4}$, y, 0. A cut (or a slab) of a CPX structure, parallel to (001) and 10-tetrahedra wide, was thus successfully located with respect to the unit cell of the En-IV phase as shown in Fig. 3 below. Successive Fourier syntheses finally revealed the atomic locations at the boundaries of the slabs. The structure thus revealed contains 124 O atoms and the cation positions in the unit cell as listed in Table 4.

For 124 O atoms, the chemical composition of specimen (1) may be expressed by the formula $Mg_{38\cdot63}Sc_{3\cdot10}Li_{1\cdot16}Si_{40\cdot07}O_{124}$.

As the number of the positions for Si in the unit cell is limited to 40 (Table 4), the excess of 0·07 Si were located together with Li at the tetrahedral positions, which we denote T, at the boundary. With this assignment of atoms, the T site remains about $\frac{1}{3}$ vacant. Mg and Sc atoms were then statistically distributed over a total of 42 M positions (Table 4);

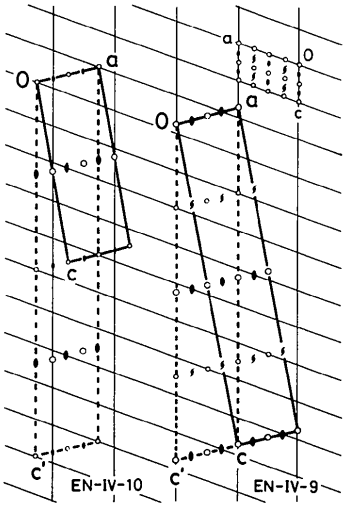

Fig. 2. The monoclinic unit cells of En-IV-10 and En-IV-9, showing their relationships to the unit cell of a C-centred clinopyroxene. The light lines trace the lattice of the clinopyroxene; the rotation axes and centres of symmetry viewed down **b** are indicated in a unit cell at the upper right corner. Heavy lines and broken lines show the B and A sets of axes, respectively. The centres of symmetry and twofold axes newly generated in the supercells are distinguished from those retained by the size of the corresponding symbols.

Table 3. *Intensity-study data*

	En-IV-10	En-IV-9	En-IV-8
Crystal size (mm)	0·25×0·15 ×0·10	0·31×0·10 ×0·06	0·35×0·25 ×0·15
μ (cm^{-1})	116·47	182·51	127·68
$2\theta_{max}$(Cu $K\alpha$) (°)	130	125	130
Number of measured reflections	3287	2673	3220
Number of reflections used	2621	1790	2557
Parameters p, q for weighting scheme*	40, 0·0029	40, 0·003	10, 0·009
R isotropic (%)	6·1	7·1	6·9
R anisotropic (%)	5·3	6·2	5·5
R_w isotropic (%)	9·0	9·7	11·5
R_w anisotropic (%)	7·8	8·8	9·3

* $w=1/(p+F_0+qF_0^2)$.

Table 4. *Number of cation positions and types of polyhedra about the cations in the unit cell of the En-*IV-10 *structure type*

	CPX slab			Boundary		
Cation	Si	M		M	M	T
Polyhedron	Tetrahedron	Octahedron		Octahedron	Trigonal-prism	Tetrahedron
No. of total positions	40	36		2	4	2
No. of distinct sites	10	8	2	1	1	1
Equipoint	4(*g*)	4(*g*)	2(*e*)	2(*d*)	4(*g*)	2(*f*)
Site symmetry	1	1	2	$\bar{1}$	1	2

Table 5. *Atomic parameters of En-IV-10 (atomic fractional coordinates are multiplied by* 10^4)

$$B_{eq} = \frac{4}{3}\sum_i\sum_j \beta_{ij}\mathbf{a}_i.\mathbf{a}_j.$$

	x	y	z	B_{eq} (Å^2)
M(1)	2500	1501 (3)	0	0·55
M(2)	2102 (2)	3501 (2)	988·7 (6)	0·52
M(3)	1690 (2)	1491 (2)	1977·5 (6)	0·54
M(4)	1234 (2)	3519 (2)	2967·8 (6)	0·49
M(5)	708 (2)	1507 (2)	3945·9 (7)	0·48
M(6)	−783 (2)	3397 (2)	4917·5 (6)	0·88
M(7)	7500	4879 (3)	0	0·78
M(8)	7093 (1)	117 (2)	987·7 (6)	0·76
M(9)	6662 (2)	4891 (2)	1973·9 (6)	0·79
M(10)	6257 (2)	129 (2)	2968·1 (6)	0·71
M(11)	5874 (2)	4891 (2)	3986·2 (6)	0·71
M(12)	5221 (4)	−31 (6)	4981·4 (2)	0·41
Si(1)	5229 (1)	3403 (1)	511·8 (4)	0·21
Si(2)	4837 (1)	1601 (1)	1481·9 (4)	0·22
Si(3)	4422 (1)	3402 (1)	2445·1 (4)	0·26
Si(4)	3994 (1)	1634 (1)	3398·8 (4)	0·33
Si(5)	3580 (1)	3217 (1)	4355·7 (4)	0·65
Si(6)	9380 (1)	1599 (1)	457·7 (4)	0·20
Si(7)	8979 (1)	3381 (1)	1425·4 (4)	0·21
Si(8)	8564 (1)	1619 (1)	2387·6 (4)	0·29
Si(9)	8064 (1)	3325 (1)	3338·0 (4)	0·46
Si(10)	7428 (1)	1644 (1)	4247·4 (4)	0·65
T	2500	1182 (39)	5000	0·81
O(1)	5987 (3)	2565 (4)	53 (1)	0·79
O(2)	3526 (3)	3449 (3)	414 (1)	0·51
O(3)	6046 (3)	4991 (4)	545 (1)	0·84
O(4)	5603 (3)	2350 (4)	1004 (1)	0·68
O(5)	3130 (3)	1557 (3)	1396 (1)	0·45
O(6)	5645 (3)	9 (4)	1534 (1)	0·64
O(7)	5209 (3)	2737 (4)	1957 (1)	0·60
O(8)	2714 (3)	3430 (3)	2374 (1)	0·48
O(9)	5213 (3)	4995 (4)	2514 (1)	0·59
O(10)	4801 (3)	2199 (4)	2900 (1)	0·68
O(11)	2276 (3)	1610 (3)	3340 (1)	0·60
O(12)	4780 (3)	35 (3)	3491 (1)	0·54
O(13)	4380 (3)	2911 (3)	3827 (1)	0·65
O(14)	1889 (3)	3249 (4)	4281 (1)	0·93
O(15)	4394 (3)	4783 (4)	4521 (1)	0·80
O(16)	4157 (3)	1990 (4)	4757 (1)	0·95
O(17)	8551 (3)	13 (4)	448 (1)	0·78
O(18)	11078 (3)	1541 (3)	569 (1)	0·44
O(19)	8627 (3)	2543 (4)	893 (1)	0·91
O(20)	8138 (3)	4953 (4)	1445 (1)	0·84
O(21)	10666 (3)	3453 (3)	1548 (1)	0·55
O(22)	8258 (3)	2282 (4)	1828 (1)	0·89
O(23)	7697 (3)	84 (4)	2442 (1)	0·84
O(24)	10244 (3)	1551 (4)	2531 (1)	0·65
O(25)	7858 (3)	2873 (4)	2751 (1)	0·88
O(26)	7169 (3)	4827 (4)	3423 (1)	0·81
O(27)	9734 (3)	3414 (3)	3520 (1)	0·56
O(28)	7359 (3)	1867 (4)	3635 (1)	0·74
O(29)	6578 (3)	174 (4)	4416 (1)	1·16
O(30)	9087 (3)	1516 (3)	4457 (1)	0·73
O(31)	6935 (3)	3237 (4)	4495 (1)	1·03

isotropic least-squares refinement, with *ORFLS* (Busing, Martin & Levy, 1962), converged to give R = 7·9%. Subsequent occupancy refinement, with constraint on chemical composition, and anisotropic refinement reduced R to 5·3%. Finally, several tests were made to locate Mg, together with Si and Li, at the T site. Trials of site-occupancy refinement and examination of the difference Fourier syntheses showed that the location of Mg at this site was unlikely. Throughout the structure analysis, neutral atomic form factors were used (*International Tables for X-ray Crystallography*, 1962). For least-squares calculations the weighting scheme used was of the form shown in Table 3. The average and maximum shifts of atomic parameters as fractions of their e.s.d.'s in the final refinement cycle are respectively 0·09 and 0·45. The atomic parameters obtained are listed in Table 5.*

The crystal structures of specimens (2) and (3) were readily determined because they are based on the principles used for specimen (1). Both structures were refined similarly to specimen (1), except that we used the least-squares program *LINUS* (Coppens & Hamilton, 1970) in the latter two cases (Table 3); maximum shifts to error were 2·0 [the occupancy of Mg at *M*(6) for specimen (2)] and 1·6 [the occupancy of Sc at *M*(10) for specimen (3)], and mean shifts to error were 0·10 [specimen (2)] and 0·09 [specimen (3)]. We give final atomic parameters in Tables 6 and 7.*

Nomenclature of subphases

As shown in Fig. 3, the crystal structure of En-IV-10 consists of slabs, parallel to (001), of a CPX structure, each slab being 10 silicate tetrahedra wide. An alternative description is that the pyroxene chains in the slab have a limited extension of 10 tetrahedra. The Arabic figure which follows En-IV represents this number of silicate tetrahedra that defines the width of the CPX slab. Similarly, the subphases denoted En-IV-9 and En-IV-8 have structures consisting of CPX slabs in which the silicate chains are 9 tetrahedra and 8 tetrahedra long, respectively. The variety in

* See deposition footnote.

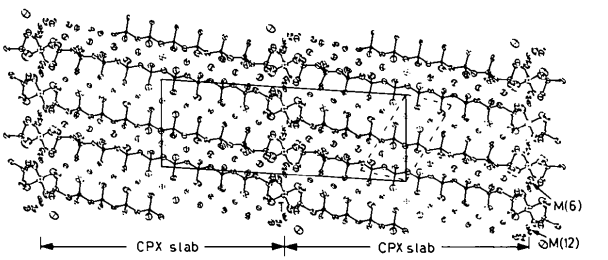

Fig. 3. The *b*-axis projection of the crystal structure of En-IV-10 bounded by approximately $y = 0$ and $y = 0·5$. The primitive unit cell is indicated, with the origin at the upper right corner and *a* axis vertical; broken lines trace the CPX subcell. The cations *T*, *M*(6), and *M*(12) locating the slab boundary are indicated. The Si–O and *T*–O bonds are shown by solid lines.

* Lists of structure factors, anisotropic thermal parameters and bond lengths (for En-IV-9 and En-IV-8) have been deposited with the British Library Lending Division as Supplementary Publication No. SUP 38996 (38 pp.). Copies may be obtained through The Executive Secretary, International Union of Crystallography, 5 Abbey Square, Chester CH1 2HU, England.

Table 6. *Atomic parameters of En-*IV-9 (*atomic fractional coordinates are multiplied by* 10^4)

$$B_{eq}=\tfrac{4}{3}\sum_i\sum_j\beta_{ij}\mathbf{a}_i.\mathbf{a}_j.$$

	x	y	z	B_{eq} (Å^2)
M(1)	2276 (3)	1499 (3)	2774·2 (5)	0·26
M(2)	1818 (3)	3514 (3)	3322·7 (5)	0·29
M(3)	1321 (3)	1477 (3)	3873·7 (5)	0·48
M(4)	756 (3)	3497 (3)	4416·3 (5)	0·21
M(5)	−767 (3)	1607 (4)	4955·0 (6)	0·68
M(6)	7272 (3)	4882 (3)	2773·5 (7)	0·79
M(7)	6786 (3)	110 (4)	3322·0 (6)	0·87
M(8)	6344 (3)	4877 (3)	3873·5 (6)	0·55
M(9)	5899 (3)	110 (3)	4437·7 (6)	0·60
M(10)	4766 (5)	5005 (8)	5006 (1)	1·40
Si (1)	4990 (3)	3392 (3)	3053·1 (5)	0·05
Si (2)	4524 (3)	1604 (3)	3586·4 (5)	0·03
Si (3)	4055 (3)	3371 (3)	4114·4 (5)	0·08
Si (4)	3600 (3)	1777 (3)	4644·1 (5)	0·29
Si (5)	9572 (2)	3395 (3)	2483·7 (5)	0·08
Si (6)	9127 (3)	1616 (3)	3019·6 (5)	0·04
Si (7)	8667 (3)	3379 (3)	3553·9 (5)	0·01
Si (8)	8129 (3)	1681 (3)	4081·0 (5)	0·21
Si (9)	7458 (3)	3354 (3)	4585·5 (5)	0·48
T	2500	3867 (3)	5000	2·31
O(1)	5758 (7)	2588 (8)	2796 (1)	0·62
O(2)	3285 (6)	3439 (8)	3006 (1)	0·32
O(3)	5790 (7)	4996 (8)	3074 (1)	0·56
O(4)	5334 (6)	2296 (7)	3319 (1)	0·11
O(5)	2826 (6)	1585 (8)	3549 (1)	0·45
O(6)	5323 (6)	16 (8)	3621 (1)	0·34
O(7)	4883 (7)	2781 (8)	3838 (1)	0·52
O(8)	2341 (6)	3395 (8)	4079 (1)	0·32
O(9)	4828 (6)	4966 (8)	4161 (1)	0·34
O(10)	4431 (7)	2111 (7)	4354 (1)	0·40
O(11)	1906 (7)	1767 (8)	4602 (1)	0·74
O(12)	4405 (7)	194 (8)	4731 (1)	0·78
O(13)	4151 (7)	2995 (8)	4866 (1)	0·68
O(14)	8757 (7)	4982 (8)	2478 (1)	0·58
O(15)	11282 (7)	3444 (9)	2541 (1)	0·67
O(16)	8803 (7)	2468 (8)	2730 (1)	0·67
O(17)	8299 (6)	44 (8)	3026 (1)	0·38
O(18)	10824 (7)	1561 (8)	3086 (1)	0·49
O(19)	8396 (7)	2702 (8)	3246 (1)	0·72
O(20)	7803 (7)	4920 (8)	3583 (1)	0·50
O(21)	10352 (6)	3446 (8)	3628 (1)	0·30
O(22)	7955 (7)	2155 (8)	3759 (1)	0·68
O(23)	7233 (6)	165 (8)	4127 (1)	0·31
O(24)	9801 (7)	1573 (8)	4176 (1)	0·46
O(25)	7411 (7)	3117 (8)	4244 (1)	0·60
O(26)	6580 (7)	4824 (8)	4678 (1)	0·92
O(27)	9114 (7)	3473 (8)	4702 (1)	0·85
O(28)	6940 (7)	1748 (9)	4719 (1)	0·96

Table 7. *Atomic parameters of En-*IV-8 (*atomic fractional coordinates are multiplied by* 10^4)

$$B_{eq}=\tfrac{4}{3}\sum_i\sum_j\beta_{ij}\mathbf{a}_i.\mathbf{a}_j.$$

	x	y	z	B_{eq} (Å^2)
M(1)	2500	1480 (2)	0	0·90
M(2)	1986 (1)	3523 (1)	1236·1 (5)	0·69
M(3)	1428 (1)	1464 (1)	2472·0 (5)	0·64
M(4)	801 (1)	3497 (1)	3692·2 (5)	0·54
M(5)	−761 (1)	1579 (1)	4900·5 (5)	0·96
M(6)	7500	4878 (2)	0	1·40
M(7)	6961 (1)	117 (2)	1233·9 (6)	1·17
M(8)	6453 (1)	4865 (1)	2471·0 (6)	0·98
M(9)	5970 (1)	113 (1)	3744·1 (6)	0·79
M(10)	4807 (2)	4987 (3)	5018 (1)	0·50
Si(1)	5173 (1)	3392 (1)	638·3 (5)	0·46
Si(2)	4662 (1)	1596 (1)	1835·1 (5)	0·45
Si(3)	4136 (1)	3372 (1)	3017·5 (5)	0·47
Si(4)	3628 (1)	1789 (1)	4204·2 (5)	0·60
Si(5)	9325 (1)	1616 (1)	564·6 (5)	0·49
Si(6)	8820 (1)	3376 (1)	1762·1 (5)	0·52
Si(7)	8223 (1)	1682 (1)	2945·6 (5)	0·55
Si(8)	7484 (1)	3352 (1)	4070·1 (5)	0·56
T	2500	3820 (1)	5000	0·30
O(1)	5970 (3)	2538 (3)	75 (1)	1·05
O(2)	3464 (3)	3456 (3)	525 (1)	0·75
O(3)	5996 (3)	4986 (3)	675 (1)	0·87
O(4)	5494 (3)	2317 (3)	1243 (1)	1·02
O(5)	2950 (3)	1559 (3)	1746 (1)	0·68
O(6)	5464 (3)	−2 (3)	1906 (1)	0·81
O(7)	5002 (3)	2780 (3)	2407 (1)	0·94
O(8)	2427 (3)	3404 (3)	2946 (1)	0·73
O(9)	4923 (3)	4965 (3)	3121 (1)	0·85
O(10)	4491 (3)	2100 (3)	3554 (1)	0·86
O(11)	1945 (3)	1747 (3)	4109 (1)	0·79
O(12)	4442 (3)	218 (3)	4402 (1)	0·83
O(13)	4186 (3)	3015 (3)	4704 (1)	0·99
O(14)	8475 (3)	36 (3)	569 (1)	0·94
O(15)	11026 (3)	1539 (3)	699 (1)	0·80
O(16)	8559 (3)	2649 (3)	1086 (1)	1·12
O(17)	7937 (3)	4931 (3)	1812 (1)	0·86
O(18)	10513 (3)	3465 (3)	1928 (1)	0·84
O(19)	8078 (3)	2157 (3)	2231 (1)	1·00
O(20)	7315 (3)	173 (3)	3043 (1)	0·75
O(21)	9886 (3)	1576 (3)	3165 (1)	0·78
O(22)	7485 (3)	3138 (3)	3320 (1)	0·71
O(23)	6606 (3)	4823 (3)	4277 (1)	1·01
O(24)	9132 (3)	3495 (3)	4325 (1)	0·81
O(25)	6984 (3)	1752 (3)	4367 (1)	0·86

structure of the En-IV series is thus basically characterized by the difference in width of the constituent CPX slabs, while the manner of combining the slabs to complete the continuity of their structures is in principle the same. Further details of the structural relationship between subphases are discussed below.

Discussion of the structure of En-IV-10

General features

The crystal structure of the En-IV-10 phase, which represents well the En-IV chemical series, is described and discussed. In subsequent paragraphs, the finite chain of 10 tetrahedra will be called a 'chain unit' of the structure. The apical bonds, which belong to the Si–**O1** family of CPX, of the constituent tetrahedra of the chain unit have nearly the same orientation as those in CPX, and point in either +**a** or −**a** directions. The terminal tetrahedra at both ends of each chain unit are linked, sharing corners, with tetrahedra which are denoted T and located at the slab boundaries. As T is on a twofold axis, it plays the role of joining the chain unit with those in adjacent slabs, resulting in the formation of a chain of infinite extension. In the infinite chain of tetrahedra thus formed, the set of the above-mentioned apical bonds of tetrahedra in every second chain unit points in the opposite direc-

Table 8. *Bond lengths* (Å) *of the En-*IV-10 *structure*

Estimated errors are ±0·003 Å for *M*–O and Si–O, and ±0·015 Å for *T*–O.

M(1)		*M*(5)		*M*(9)		Si(1)		Si(6)	
–O(17)*a* ×2	2·018	–O(12)*b*	1·994	–O(21)*f*	2·045	–O(3)	1·588	–O(17)	1·592
–O(18)*c* ×2	2·097	–O(14)	2·066	–O(8)*i*	2·046	–O(2)	1·613	–O(18)	1·613
–O(2) ×2	2·230	–O(29)*b*	2·082	–O(20)	2·052	–O(1)	1·639	–O(19)	1·633
Av.	2·115	–O(30)*c*	2·118	–O(9)	2·059	–O(4)	1·640	–O(1)*d*	1·640
		–O(27)*c*	2·198	–O(7)	2·329	Av.	1·620	Av.	1·620
M(2)		–O(11)	2·270	–O(22)	2·774				
–O(3)*f*	2·009	Av.	2·121	Av.	2·218	Si(2)		Si(7)	
–O(20)*f*	2·041					–O(6)	1·589	–O(20)	1·590
–O(21)*c*	2·087	*M*(6)		*M*(10)		–O(5)	1·614	–O(21)	1·608
–O(2)	2·110	–O(15)*f*	1·931	–O(23)	2·022	–O(7)	1·646	–O(22)	1·629
–O(5)	2·219	–O(31)*g*	1·980	–O(11)*j*	2·035	–O(4)	1·652	–O(19)	1·633
–O(18)*c*	2·243	–O(30)*c*	2·063	–O(12)	2·042	Av.	1·625	Av.	1·615
Av.	2·118	–O(16)*g*	2·118	–O(24)*b*	2·083				
		–O(15)*g*	2·295	–O(10)	2·274	Si(3)		Si(8)	
M(3)		–O(31)*c*	2·382	–O(28)	2·534	–O(9)	1·587	–O(23)	1·583
–O(6)*b*	2·000	Av.	2·128	Av.	2·165	–O(8)	1·611	–O(24)	1·611
–O(23)*b*	2·059					–O(10)	1·642	–O(22)	1·632
–O(24)*c*	2·082	*M*(7)		*M*(11)		–O(7)	1·656	–O(25)	1·640
–O(5)	2·136	–O(2)*h* ×2	2·051	–O(26)	2·007	Av.	1·624	Av.	1·617
–O(8)	2·200	–O(3) ×2	2·070	–O(14)*i*	2·026				
–O(21)*c*	2·257	–O(1) ×2	2·485	–O(15)	2·068	Si(4)		Si(9)	
Av.	2·122	Av.	2·202	–O(27)*f*	2·187	–O(12)	1·596	–O(26)	1·585
				–O(31)	2·198	–O(11)	1·618	–O(27)	1·624
M(4)		*M*(8)		–O(13)	2·259	–O(13)	1·635	–O(25)	1·636
–O(9)*f*	1·995	–O(18)*b*	2·045	Av.	2·124	–O(10)	1·662	–O(28)	1·666
–O(26)*f*	2·064	–O(5)*j*	2·049			Av.	1·628	Av.	1·628
–O(27)*c*	2·116	–O(17)	2·063	*M*(12)					
–O(11)	2·158	–O(6)	2·069	–O(16)*k*	1·932	Si(5)		Si(10)	
–O(8)	2·188	–O(4)	2·407	–O(16)	2·105	–O(14)	1·597	–O(29)	1·596
–O(24)*c*	2·259	–O(*i*9)	2·589	–O(30)*l*	2·110	–O(16)	1·600	–O(31)	1·625
Av.	2·130	Av.	2·204	–O(30)*b*	2·161	–O(15)	1·621	–O(30)	1·637
				–O(29)	2·057	–O(13)	1·676	–O(28)	1·666
				–O(29)*k*	2·422	Av.	1·624	Av.	1·631
				Av.	2·131				
				T					
				–O(16) ×2	1·867				
				–O(29)*k* ×2	2·122				
				Av.	1·995				

Symmetry code

(*a*) $1-x,-y,-z$ (*e*) $\frac{1}{2}-x,\ y,-z$ (*i*) $\frac{1}{2}+x,\ 1-y,\ z$ (*m*) $1-x,\ 1-y,\ 1-z$

(*b*) $-\frac{1}{2}+x,-y,\ z$ (*f*) $-\frac{1}{2}+x,\ 1-y,\ z$ (*j*) $\frac{1}{2}+x,-y,\ z$ (*n*) $1+x,\ y,\ z$

(*c*) $-1+x,\ y,\ z$ (*g*) $\frac{1}{2}-x,\ y,\ 1-z$ (*k*) $1-x,-y,\ 1-z$ (*p*) $\frac{3}{2}-x,\ \frac{1}{2}-y,\ \frac{1}{2}-z$

(*d*) $\frac{3}{2}-x,\ y,-z$ (*h*) $1-x,\ 1-y,-z$ (*l*) $\frac{3}{2}-x,\ y,\ 1-z$ (*r*) $1-x,-\frac{1}{2}+y,\ \frac{1}{2}-z$

tion with respect to those of the first (Fig. 3). Consequently, the chain by itself has a periodicity corresponding in length to 22 tetrahedra (55·4 Å). When we look at the structure down **a**, we note that the chain of tetrahedra is not single but, in fact, multiple. A pair of chain units, which are in the same slab and in a plane parallel to (201), are linked together at their ends by a pair of tetrahedra, *T*, as shown in Fig. 8, thus forming a loop consisting of 22 tetrahedra in the same slab.

The above structure of En-IV-10 now yields the following structure formula in which charge is balanced for 124 O atoms:

$$(Mg_{38\cdot63}Sc_{3\cdot10})_{\Sigma=41\cdot73}[(Li_{1\cdot16}Si_{0\cdot07})Si_{40}]_{\Sigma=41\cdot23}O_{124}.$$

The primitive unit cell of this material contains one formula unit. This formula shows that the *T* sites in the unit cell contain 1·16 Li and 0·07 Si. As there are two *T* sites per cell, this situation implies that each *T* site is 38·5% vacant. Similarly, a total of 0·27 vacancies per cell are distributed over the 42 positions for Mg and Sc. The chemical formula thus expressed is very close to the following idealized formula having the form for a metasilicate:

$$(M^{2+}_{37\cdot33}Sc_4)_{\Sigma=41\cdot33}(Li_{1\cdot33}Si_{40})_{\Sigma=41\cdot33}O_{124}.$$

We may then regard the substitution scheme underlying the chemistry of En-IV-10 as being basically of the form $3Mg+Si \rightleftarrows 3Sc+Li$. As will be shown later, the chemistry of the whole series of En-IV is characterized by the new substitution scheme above.

Characteristics of the CPX slabs

The structure of the CPX slab (Fig. 4) is closely similar to the structure of a *C*-centred clinopyroxene such as high clinohypersthene (Smyth, 1974) or $LiScSi_2O_6$ (Hawthorne & Grundy, 1977); the silicate chain elements are in an *O*-rotated configuration (Thompson, 1970). In Table 8, which gives bond lengths, the four independent Si–O bonds of each tetrahedron are listed so that they correspond to those commonly denoted for CPX structures in the following way: those in the first and second lines correspond to Si–**O2** and Si–**O1**, respectively, and those in the last two lines to Si–**O3** bridge bonds. The mode of scattering of bond lengths in each tetrahedron shares a feature with those of the tetrahedra of CPX structures: the bond corresponding to Si–**O2** is shortest and that corresponding to Si–**O1** is second shortest (Clark, Appleman & Papike, 1969).

Table 9. *Angle (°) subtended by a pair of tetrahedral bonds at each bridge O atom of the silicate chains*

En-IV-10		En-IV-8	
Tk–O(29)–Si(10)	118·2	*Tm*–O(23)–Si(8)	117·2
Si(10)–O(28)–Si(9)	125·0	Si(8)–O(22)–Si(7)	125·5
Si(9)–O(25)–Si(8)	135·5	Si(7)–O(19)–Si(6)	137·6
Si(8)–O(22)–Si(7)	140·4	Si(6)–O(16)–Si(5)	142·2
Si(7)–O(19)–Si(6)	142·0	Si(5)*d*–O(1)–Si(1)	142·8
Si(6)*d*–O(1)–Si(1)	141·9	Si(1)–O(4)–Si(2)	139·9
Si(1)–O(4)–Si(2)	140·8	Si(2)–O(7)–Si(3)	135·4
Si(2)–O(7)–Si(3)	138·5	Si(3)–O(10)–Si(4)	128·2
Si(3)–O(10)–Si(4)	135·1	Si(4)–O(13)–*T*	102·5
Si(4)–O(13)–Si(5)	128·4	Estimated errors: ±0·2° for Si–O–Si, and ±0·3° for Si–O–*T*	
Si(5)–O(16)–*T*	103·5		
Estimated errors: ±0·1° for Si–O–Si, and ±0·2° for Si–O–*T*			
En-IV-9		En-IV-9	
Tm–O(26)–Si(9)	116·4	Si(5)*p*–O(1)–Si(1)	142·5
Si(9)–O(25)–Si(8)	125·4	Si(1)–O(4)–Si(2)	139·2
Si(8)–O(22)–Si(7)	137·2	Si(2)–O(7)–Si(3)	135·6
Si(7)–O(19)–Si(6)	141·5	Si(3)–O(10)–Si(4)	128·9
Si(6)–O(16)–Si(5)	142·6	Si(4)–O(13)–*T*	104·9
Estimated errors: ±0·5° for Si–O–Si, and ±0·6° for Si–O–*T*			

There is, however, a marked difference in Si–O–Si bond angle between the chain units of the En-IV-10 slab and the silicate chains in CPX. While the bond angle at the bridge O atom is constant for a given tetrahedral chain in a CPX structure, those in the chain unit of En-IV-10 show a spectrum of values. The variation is such that the angle at the bridge O atom, O(1), in the central region of the chain unit has a maximum value of 142·0° but the angles gradually decrease as the locations of the bridge O atoms approach both ends of the chain unit, *e.g.* at O(13) the angle has a value as small as 128·4° (Fig. 5*a* and Table 9). The chain unit is in fact highly stretched in the region of its central portion, the angle corresponding to **O3–O3–O3** being 175·5° at O(1). This value is to be compared with the relatively high values of 172·4° reported for clinohypersthene, $Mg_{0.31}Fe_{0.67}Ca_{0.015}SiO_3$, at 1098 K (Smyth, 1974) and 175·6 (1)° found for $LiScSi_2O_6$ (Hawthorne & Grundy, 1977), both having space group $C2/c$; the highest value of 179·3° has been observed for the *A* chain in orthoferrosilite, $FeSiO_3$ (space group *Pbca*), at 1253 K (Sueno, Cameron & Prewitt, 1976). The values of the **O3–O3–O3** angles found for En-IV-10 likewise gradually decrease as the locations of the bridge O atoms approach both ends of the chain unit, giving an average value of 162°.

In general, the configurations of metasilicate chains, such as those of the pyroxenoid series, sensibly vary to adjust dimensional misfit between the chain and the arrays of octahedra which they flank. In the case of En-IV-10, which is stable above 1673 K, the array of octahedra, each containing on average 92·0% Mg and 7·4% Sc, would be of critical dimensions to allow the continuous extension of a

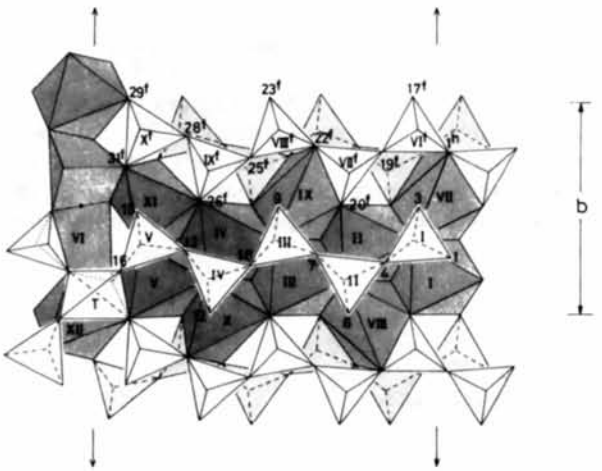

Fig. 4. The links of polyhedra approximately in the lower half of the *B*-centred cell of the En-IV-10 structure [projection on (201) of the primitive cell]. The notations of the cation polyhedra and the silicate tetrahedra are indicated by Roman figures. To avoid confusion, the notations of only the basal O atoms are given by Arabic figures; those for the apical O atoms may readily be identified in Table 8. The twofold axis on the right passes through *M*(1)(=I) and *M*(7) (=VII), and that on the left, *T*.

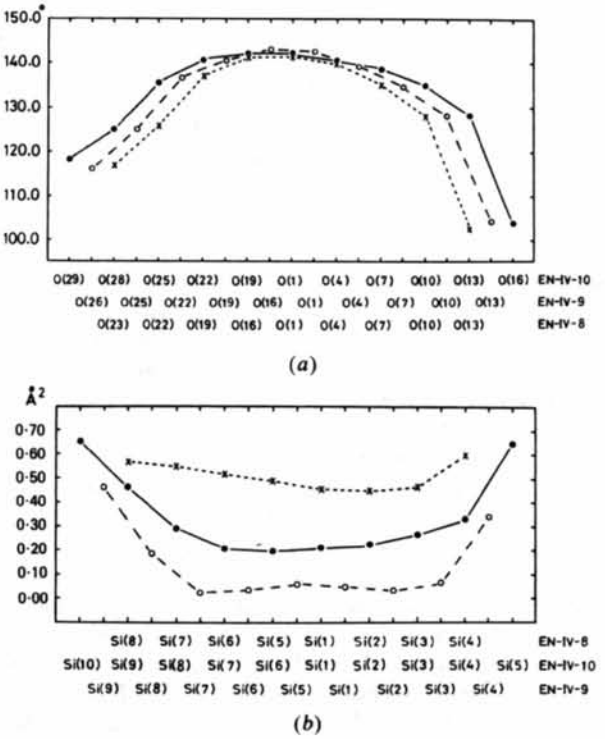

Fig. 5. (*a*) The mode of variation in the Si–O–Si angle of the finite silicate chains in the En-IV-10, En-IV-9, and En-IV-8 structures. The bridge O atoms in each chain are indicated along the horizontal axis successively from that at one end of the chain through to that at the other. (*b*) The variation in isotropic temperature factor (*B*) of the Si atoms. The Si atoms are indicated along the horizontal axis in the same fashion as the bridge O atoms in (*a*).

Table 10. *Atomic contents in the cation sites of the En-IV structures*

Atomic site	Equi-point	Corresponding site in pyroxene	Contents Mg	Sc		
En-IV-10						
$M(1)$	2(*e*)		0·902 (6)	0·092 (8)		
$M(2)$	4(*g*)		0·907 (4)	0·087 (6)		
$M(3)$	4(*g*)	$M(1)$	0·897 (4)	0·099 (6)		
$M(4)$	4(*g*)		0·897 (4)	0·105 (6)		
$M(5)$	4(*g*)		0·836 (4)	0·162 (6)		
$M(12)$	2(*b*)		0·754 (6)	0·243 (12)		
$M(7)$	2(*e*)		0·979 (6)	0·008 (12)		
$M(8)$	4(*g*)		0·973 (4)	0·017 (6)		
$M(9)$	4(*g*)	$M(2)$	0·963 (4)	0·029 (6)		
$M(10)$	4(*g*)		0·962 (4)	0·031 (6)		
$M(11)$	4(*g*)		0·950 (4)	0·045 (6)		
$M(6)$	4(*g*)		0·960 (4)	0·030 (6)		
T	2(*f*)		0·58 Li	0·035 Si		
En-IV-8						
$M(1)$	2(*e*)		0·821 (4)	0·163 (2)		
$M(2)$	4(*g*)	$M(1)$	0·831 (3)	0·141 (2)		
$M(3)$	4(*g*)		0·849 (3)	0·127 (2)		
$M(4)$	4(*g*)		0·805 (3)	0·191 (2)		
$M(10)$	2(*b*)		0·305 (6)	0·636 (2)		
$M(6)$	2(*e*)		0·965 (4)	0·032 (2)		
$M(7)$	4(*g*)	$M(2)$	0·907 (3)	0·054 (2)		
$M(8)$	4(*g*)		0·910 (3)	0·066 (2)		
$M(9)$	4(*g*)		0·889 (3)	0·093 (2)		
$M(5)$	4(*g*)		0·908 (4)	0·078 (2)		
T	2(*f*)		0·67 Li			
En-IV-9			Mg	Co	Sc	Li
$M(1)$	8(*f*)		0·806 (8)	0·054 (3)	0·140 (5)	—
$M(2)$	8(*f*)	$M(1)$	0·784 (8)	0·179 (3)	0·000 (5)	—
$M(3)$	8(*f*)		0·760 (8)	0·139 (3)	0·096 (5)	—
$M(4)$	8(*f*)		0·824 (8)	0·078 (3)	0·098 (5)	—
$M(10)$	4(*b*)		0·312 (8)	0·324 (3)	0·354 (5)	
$M(6)$	8(*f*)		0·779 (8)	0·123 (3)	0·035 (5)	0·063
$M(7)$	8(*f*)	$M(2)$	0·743 (9)	0·097 (4)	0·107 (5)	0·053
$M(8)$	8(*f*)		0·858 (8)	0·073 (3)	0·069 (5)	0·000
$M(9)$	8(*f*)		0·704 (8)	0·040 (4)	0·226 (5)	0·030
$M(5)$	8(*f*)		0·646 (8)	0·145 (3)	0·007 (8)	0·202
T	4(*e*)		0·244 Si			

pyroxene chain along it. The En-IV-10 structure now revealed shows that the pyroxene chains in the structure are dimensionally adjusted to the octahedral array by limiting their extension to 10 tetrahedra and adding extra tetrahedra, T, at both ends to retain the continuity of the chain structure. Compared with the pyroxene structures in which the ratio of the number of octahedra to the number of tetrahedra, both defining their c periodicity, is 2:2 [two successive $M(1)$ octahedra define the c length], the corresponding ratio in En-IV-10 is 10:11. We may consider that the addition of extra tetrahedra provides pyroxene chains with a relaxation from the misfitting between the octahedral arrays and the chains which are otherwise hindered from extending continuously. The above mode of variation in the Si–O–Si angle would be the result of such a relaxation taking place to form the structure.

Among octahedral cations, $M(1)\sim M(5)$ belong to **M1**, while $M(7)\sim M(11)$ to **M2**. Of these, $M(9)$ and $M(10)$ share an additional neighbour [the bridge O atom O(25)] at distances of 2·922 and 2·912 Å, respectively. The coordinations of these two cations may hence be regarded as sevenfold (in Fig. 4, they are expressed as sixfold). The Sc atoms are mainly distributed over the **M1** octahedra. As given in Table 10, there is a trend that the Sc contents in the octahedra increase as the positions of the octahedra approach the slab boundaries.

Constitution of the boundaries

Each boundary of the slabs is composed of a centrosymmetric pair of layers, parallel to (001), consisting of O atoms which are arranged very closely in a closest-packed fashion. In the voids formed by the O layers, cations are distributed so that their neighbouring O atoms form octahedra, trigonal prisms or tetrahedra. The way in which these polyhedra are linked to form a layer of polyhedra is illustrated in Fig. 6.

In the octahedron denoted $M(12)$, cations are statistically located at a centrosymmetric pair of split positions, the separation being 0·438 (1) Å. The Sc contents in this octahedron show a value which is the greatest in the structure (Table 10). The octahedron plays the role of joining together those about **M1** of adjacent slabs. The trigonal prism denoted $M(6)$ contains mostly Mg. Its pyramidal faces are in fact not exactly coplanar. This polyhedron plays the role of joining together those about **M2** in adjacent slabs.

The tetrahedron, which is the one we denoted T, has two further neighbours, O(14) and O(14)g, related to each other by twofold rotation, at the same distance of 2·695 Å. Their locations are such that they form with the four O atoms about T a distorted octahedron. The tetrahedron is thus a specific tetrahedron which is formed from an octahedron; we may regard the fourfold coordination as being the result of a shift of the cation otherwise coordinated octahedrally.

Within the estimated error of ±0·015 Å, the mean T–O length of 1·995 Å (Table 8) agrees well with an Li–O distance of 1·97 Å (Shannon, 1976). The temperature factors, which are relatively small for the atoms near the centre of the slabs, increase as the locations of the atoms approach the boundaries

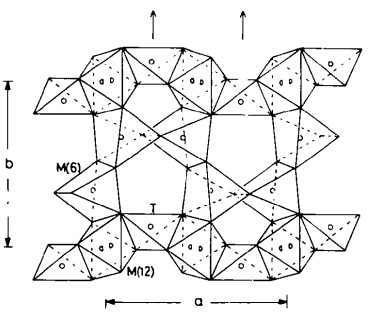

Fig. 6. The links of polyhedra at the CPX boundary. The split positions in $M(12)$ are schematically indicated.

(Table 5 and Fig. 5*b*). This trend is probably due to the effect that the closer the atomic locations are to the boundaries, the more the static disorder of the atoms increases. The relatively large error associated with *T*–O seems to be related to such an effect in addition to the low occupancy of Li at the *T* site.

Chemical composition

The En-IV-9 and En-IV-8 subphases share every structural feature with En-IV-10; *i.e.* their CPX slabs have structural characteristics which are similar to those of the CPX slabs of En-IV-10, and the constitutions of the boundaries of their slabs are in principle the same as that of En-IV-10. The difference between these subphases is basically in the width of the CPX slabs. The structural formulae of En-IV-9 and En-IV-8 can therefore be expressed as in the case of En-IV-10. In Table 11, we give for each subphase (1) the number of available atomic sites in the unit cell (half cell for the case of En-IV-9), (2) the number of cations when we assume that the ratio $M:(T+\mathrm{Si}):\mathrm{O}=1:1:3$ and (3) the number of cations based on the observed chemical composition given in Table 1.

The En-IV phases in which Co, Mn, or Zn were doped likewise crystallized in three different structure types depending upon the Sc contents in the crystals. Although crystals were available which were free from these divalent atoms and had the En-IV-9 type, we used a Co-doped En-IV-9 for structure analysis because we came across a relatively good piece of crystal having this structure type from Co-doped specimens. As will be observed in Table 11, the *T* site of this particular En-IV-9 contains only Si with an atomic occupancy of 0·244. Although trials were made of assigning Li to this site in addition to the Si atoms and refining its occupancy with least-squares calculations, the results converged to zero for the occupancy of Li. In this particular case, we therefore distributed Li over the cation sites which belong to **M2** and refined their occupancies, with total Li in the unit cell constrained to the observed Li contents (Table 1). The smaller occupancy of Si compared with the case in which *T* is occupied by Li seems to suggest that the atomic occupancy allowed for the *T* site varies depending upon the charge of the atoms. Our study on the Sc series of En-IV, which is chemically simpler than the series now considered, has revealed that this is really the case [see part II (Takéuchi, Mori, Kudoh & Ito, 1984)]. The *T*–O lengths of this structure have a mean value of 1·990 (15) Å which is evidently longer for pure Si–O. If we assume *T*–O = 1·66 Å when *T* is fully occupied by Si, the *T*–O length, when *T* is vacant, is calculated to be 2·09 Å from the above-mentioned occupancy of Si and observed mean *T*–O length.

With the exception of this En-IV-9 crystal, the structural formulae of En-IV-10 and En-IV-8 are close to the ideal form of metasilicate in which the substitution taking place is of the form $3\mathrm{Mg}+\mathrm{Si}\rightleftarrows 3\mathrm{Sc}+\mathrm{Li}$. The chemical formula of En-IV may therefore be expressed well by an idealized general form:

$$[\mathrm{Mg}_{1-12/x}\mathrm{Sc}_{12/x}][\mathrm{Li}_{4/x}\mathrm{Si}_{1-4/x}]\mathrm{O}_3$$

or

$$[\mathrm{Mg}_{(x-12)/3}\mathrm{Sc}_4][\mathrm{Li}_{4/3}\mathrm{Si}_{(x-4)/3}]\mathrm{O}_x.$$

Putting $x=124$, 112 or 100, we obtain the formulae for En-IV-10, En-IV-9, or En-IV-8, respectively. The symbols of subphases may be represented by a general form of En-IV-*N*. Although subphases having values of *N* of other than 8, 9, and 10 have not yet been found, we may assume hypothetical cases such as 11, 12, 13, or even higher. In terms of *N*, the value of *x* in the above formulae is given by $x=12N+4$.

Table 11. *Contents in the cation sites M and tetrahedral site T (for details, see text)*

	M	*T*	Si	O
En-IV-10				
(1)	42	2	40	124
(2)	37·33 Mg, 4 Sc	1·33 Li	40	124
(3)	38·63 Mg, 3·10 Sc	1·16 Li 0·07 Si	40	124
En-IV-9				
(1)	38	2	36	112
(2)	33·33 Mg, 4 Sc	1·33 Li	36	112
(3)	28·246 Mg, 3·814 Sc 4·36 Co, 1·396 Li	0·486 Si	36	112
En-IV-8				
(1)	34	2	32	100
(2)	29·33 Mg, 4 Sc	1·33 Li	32	100
(3)	28·40 Mg, 4·62 Sc	1·33 Li	32	100

Structural relationship

In Fig. 7, the structures of En-IV-10 and En-IV-8, each projected on (201), are compared with that of En-IV-9 projected on (101). In the former two cases, we can trace in every slab the loops composed of $2(N+1)$ tetrahedra as we mentioned previously. In the latter case, however, longer loops are formed, each being composed of $4(N+1)$ tetrahedra and extending over two successive slabs. Thus, in general, the structural series of En-IV-*N* can be classified into two categories: (1) *N even*, having space group $P2/a$ and loops of $2(N+1)$ tetrahedra, and (2) *N odd* ($N\geq 3$), having space group $I2/a$ and loops of $4(N+1)$ tetrahedra. These differences between (1) and (2) simply originate from the following geometrical characteristics inherent to the '*finite*' pyroxene chains *N* tetrahedra long. Namely, if *N* is even, the direction of Si–**O2** of the tetrahedron at one end of the chain is of opposite sense with respect to that of Si–**O2** of the tetrahedron at the other. While, if *N* is odd, they are of the same sense (this situation can be readily observed when we consider an ideally stretched pyroxene chain). Such a difference gives rise to a

difference in relative level, along **b**, of the tetrahedra T (Fig. 7) that connect chain units when constructing an En-IV structure from cuts of a CPX structure as described below.

Consider a C-centred CPX, its unit cell containing $4\times M\mathrm{SiO_3}$. Suppose that the structure is cut, parallel to $(10\bar{1})$ and passing through M, into slabs each containing silicate chains N tetrahedra long. Then, the slab will have a chemical composition $4\times M_N\mathrm{Si}_N\mathrm{O}_{3N+1}$ or $M_{4N}\mathrm{Si}_{4N}\mathrm{O}_{4(3N+1)}$. If these slabs are juxtaposed in parallel positions so that each is related to its adjacent ones by a glide (or a slip) of **a**/2, the O atoms of the terminal tetrahedra of the chain units form at each boundary a set of eight polyhedra including two tetrahedra as shown in Fig. 6. Since four cations are available at the boundary (they were located in the cut planes of a pair of the CPX cuts that form the boundary), we may add up to four cations including two tetrahedral cations; thus the structure type of En-IV-N is constructed.

The above procedure for forming the structure is for the cases in which the values of N are even. If odd, the CPX slabs must be so juxtaposed that each is related to its adjacent slab by a glide not of **a**/2 but of **b**/2. In both cases, the procedures for constructing En-IV-N structures preserve the n-glide planes of the original CPX structure as a-glide planes in the resulting structure; some of the twofold axes in the original CPX structure are retained in the cases of even N, while some of the twofold screw axes are retained if N is odd (Fig. 2).

In general, a glide (or a slip) can be regarded as a twin operation for the twinning on the unit-cell scale (or cell-twinning) (Ito, 1950; Takéuchi, 1978). Therefore, the above features of the En-IV-N structures may well be described as being built up of a regular repetition of cell-twinnings of a CPX structure with a glide of either **a**/2 or **b**/2 as twin operation (Fig. 8).One of the marked features of the structural series now considered is that the extension of twin individuals (slab width) varies depending upon the atomic ratio, Sc/Mg; the lower the ratio, the longer is the extension. This relation means that the smaller the Sc content, the less frequently may take place the cell-twinning to effect the relaxation of the CPX chains as mentioned previously. The En-IV series thus provides a new example of '*tropochemical cell-twinning*'. This terminology has been introduced (Takéuchi, 1978; Takéuchi *et al.*, 1979) to denote a specific class of cell-twinning which assumes a vehicle

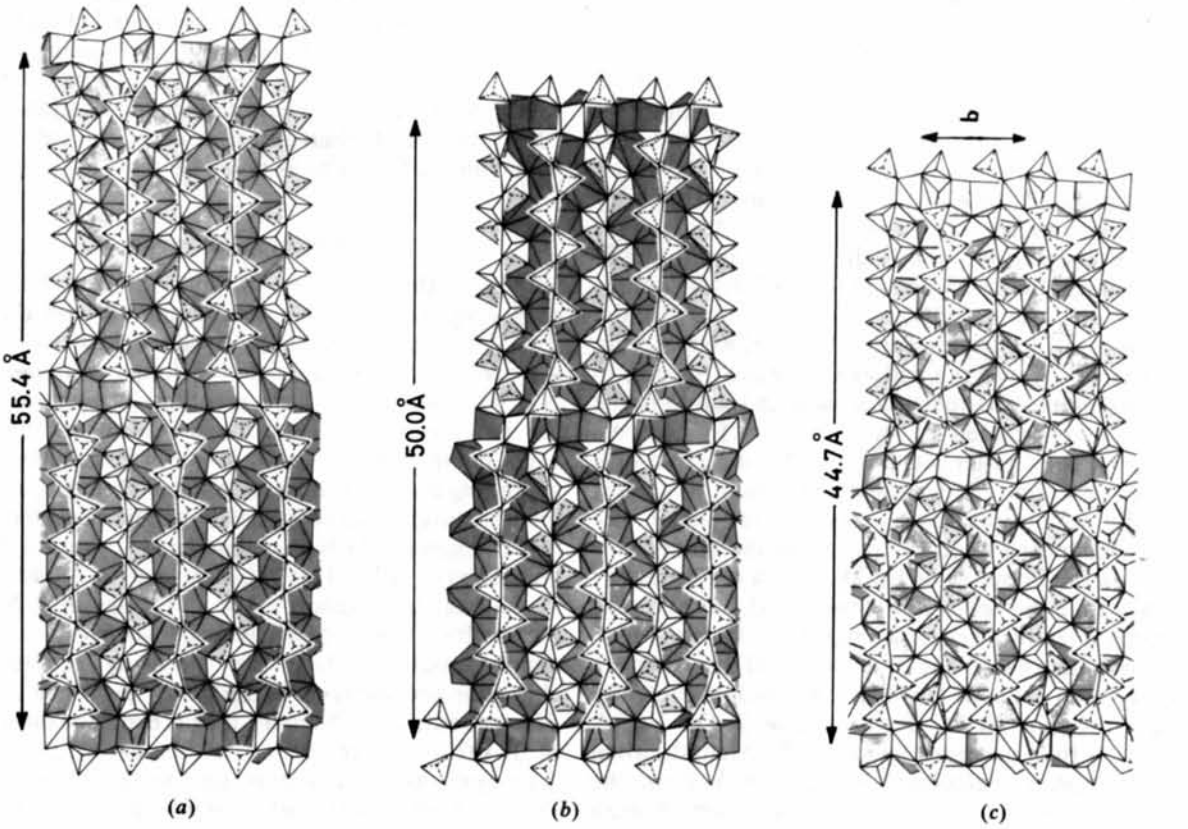

Fig. 7. Comparison of the structures of (*a*) En-IV-10, (*b*) En-IV-9, and (*c*) En-IV-8, each being projected on the (201) plane of the primitive cell. Note that each loop consisting of silicate tetrahedra and T's in En-IV-9 is formed in a way which is different from those of En-IV-10 and En-IV-8.

of changing chemical composition to yield the series of structures of the phases in a chemical system. Any phase of the structural series is neither a polymorphic form nor a polytypic variant of another because a specific range of chemical composition, though very small, is essentially associated with each phase.

The known chemical series characterized by such a cell-twinning share the following features with respect to the cations involved in substitution: a cation species, M', that substitutes for M in a chemical phase has (1) a valence state which is different from that of M, and (2) an ionic radius which is slightly different from that of M. In addition, M is of moderately large size and may have different types of coordination polyhedra about it. Thus the substitutions of Sc for Mg, Bi for Pb, and Mn^{3+} for Mn^{2+} are essential to characterize the En-IV, PbS–Bi_2S_3 (Takéuchi *et al.*, 1979), and pinakiolite series (Takéuchi *et al.*, 1978), respectively. Another example would perhaps be found in a chemical series in which the substitution of Y for Ca is involved.

Part of the crystal syntheses were carried out under the supervision of Professor O. J. Kleppa, Materials Research Laboratory of the University of Chicago, funded by the National Science Foundation; we are grateful to him for his warm encouragement extended particularly to the late Dr Jun Ito. We also thank Dr Ian M. Steele for his electron-microprobe analyses. The structural study of En-IV was supported by Grant-in-Aid for Scientific Research 242016 of the Ministry of Education of Japan. Computations were carried out on a HITAC 8800/8700 computer at the Computer Centre of the University of Tokyo.

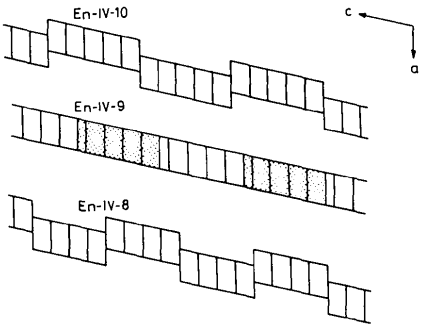

Fig. 8. Comparison of the En-IV-10, En-IV-9, and En-IV-8 structures, each being expressed by a regular repetition of slip of a block of CPX cells. The stippled blocks for En-IV-9 indicate that they are displaced by $b/2$ with respect to others.

References

BUSING, W. R., MARTIN, K. O. & LEVY, H. A. (1962). *ORFLS.* Report ORNL-TM-305. Oak Ridge National Laboratory, Tennessee.

CLARK, J. R., APPLEMAN, D. E. & PAPIKE, J. J. (1969). *Mineral Soc. Am. Spec. Pap.* **2**, 31–54.

COPPENS, P. & HAMILTON, W. C. (1970). *Acta Cryst.* A**26**, 71–83.

HAWTHORNE, F. C. & GRUNDY, H. D. (1977). *Can. Mineral.* **15**, 50–58.

International Tables for X-ray Crystallography (1962). Vol. III, pp. 201–209. Birmingham: Kynoch Press.

ITO, J. & STEELE, I. M. (1976). Geological Society of America, Annual Meeting, Denver, Abstr. pp. 937–938.

ITO, T. (1950). *X-ray Studies on Polymorphism.* Tokyo: Maruzen.

MURAKAMI, T., TAKÉUCHI, Y. & YAMANAKA, T. (1984). *Z. Kristallogr.* In the press.

SHANNON, R. D. (1976). *Acta Cryst.* A**32**, 751–767.

SMYTH, J. R. (1974). *Am. Mineral.* **59**, 1069–1082.

SMYTH, J. R. & BURNHAM, C. W. (1972). *Earth Planet. Sci. Lett.* **14**, 183–187.

SUENO, S., CAMERON, M. & PREWITT, C. T. (1976). *Am. Mineral.* **61**, 38–53.

TAKÉUCHI, Y. (1978). *Recent Progress of Natural Sciences in Japan.* Vol. 3, pp. 153–172. Science Council of Japan.

TAKÉUCHI, Y., HAGA, N., KATO, T. & MIURA, Y. (1978). *Can. Mineral.* **16**, 475–485.

TAKÉUCHI, Y., KUDOH, Y. & ITO, J. (1977). *Proc. Jpn Acad.* **53**, 60–63.

TAKÉUCHI, Y., MORI, H., KUDOH, Y. & ITO, J. (1984). *Acta Cryst.* B**40**, 126–132.

TAKÉUCHI, Y., OZAWA, T. & TAKAGI, J. (1979). *Z. Kristallogr.* **150**, 75–84.

THOMPSON, J. B. (1970). *Am. Mineral.* **55**, 292–293.

WUENSCH, B. J. & PREWITT, C. T. (1965). *Z. Kristallogr.* **122**, 24–59.